

Project No: 603502

DACCIWA

"Dynamics-aerosol-chemistry-cloud interactions in West Africa"

Deliverable

D5.5 Model evaluation

<u>Due date of deliverable:</u>	30/11/2018		
<u>Completion date of deliverable:</u>	06/12/2018		
Start date of DACCIWA project:	1 st December 2013	Project duration:	60 months
Version:	[V1.0]		
File name:	[D5.5_Model_evaluation_DACCIWA_v1.0.pdf]		
Work Package Number:	5		
Task Number:	5		
<u>Responsible partner for deliverable:</u>	ECMWF		
Contributing partners:	UREAD		
Project coordinator name:	Prof. Dr. Peter Knippertz		
Project coordinator organisation name:	Karlsruher Institut für Technologie		

Dissemination level		
PU	Public	x
PP	Restricted to other programme participants (including the Commission Services)	
RE	Restricted to a group specified by the consortium (including the Commission Services)	
CO	Confidential, only for members of the consortium (including the Commission Services)	

Nature of Deliverable		
R	Repo1	x
P	Prototype	
D	Demonstrator	
O	Other	

Copyright

This Document has been created within the FP7 project DACCIWA. The utilization and release of this document is subject to the conditions of the contract within the 7th EU Framework Programme. Project reference is FP7-ENV-2013-603502.

DOCUMENT INFO**Authors**

Author	Beneficiary Short Name	E-Mail
Peter Hill	UREAD	p.g.hill@reading.ac.uk
Angela Benedetti	ECMWF	angela.benedetti@ecmwf.int
Anke Kniffka	KIT	anke.kniffka@kit.edu
Christine Chiu	UREAD	c.j.chiu@reading.ac.uk
Peter Knippertz	KIT	peter.knippertz@kit.edu

Changes with respect to the DoW

Issue	Comments

Dissemination and uptake

Target group addressed	Project internal / external
Scientific community	Internal and external

Document Control

Document version #	Date	Changes Made/Comments
V0.1	24.10.2018	Template with basic structure
V0.2	06.11.2018	First draft
V0.3	15.11.2018	Version with input of all authors for approval by the General Assembly
V1.0	06.12.2018	Final version approved by the General Assembly

Table of Contents

1	Introduction	5
2	Observations of cloud and aerosol radiative effects	5
2.1	Cloud radiative effects	5
2.2	Aerosol radiative effects.....	9
3	Evaluation of model radiation	12
3.1	DACCIWA campaign forecasts	12
3.2	Global atmospheric models.....	13
3.3	Further analysis of climate models.....	15
4	Effect of radiative processes on circulation	17
4.1	Energy budget analysis.....	17
4.2	Effect of SW irradiance perturbations on regional precipitation and circulation	18
5	Summary and conclusions	19
6	References	20

1 Introduction

Understanding of cloud radiative effects (CREs) in the southern West Africa region is currently limited. The complex cloud climatology with frequent multilayer clouds in this region (Stein et al., 2011) makes it difficult to identify cloud types and to attribute radiative effects to different cloud regimes. A lack of surface-based cloud observations (Knippertz et al., 2015a) and uncertain aerosol–cloud interactions (Knippertz et al., 2015b) further limit understanding of clouds in this region.

Compared to CRE, direct aerosol direct radiative effects (DARE) are perhaps even less well understood over this region. While this lack of understanding is partly due to a lack of surface-based aerosol measurements, the prevalence of cloud in this region poses additional challenges in measuring aerosol properties and quantifying ADRE. These challenges include infrequent satellite aerosol retrievals, since the retrieval methods require clear-sky conditions to avoid signal contaminations from clouds. Since ADRE strongly depends on surrounding cloud conditions, which are uncertain themselves, it is even more challenging to quantify ADRE than CRE.

Within the DACCIWA project, we have estimated cloud and aerosol radiative effects using multiple-satellite dataset built from Task 5.1 and 5.3, evaluated against field campaign data in Task 5.2 and 5.4. Combining these with simulations from operational Numerical Weather Prediction (NWP) models and climate models (in collaboration with WP7), we can develop a new understanding of the interactions and potential feedbacks between cloud and aerosol radiative effects and atmospheric circulation across various temporal and spatial scales.

The main objective of the report is 1) to quantify the occurrence of various cloud types and their associated radiative effects in the DACCIWA region during the monsoon season; 2) to report aerosol direct radiative effects; and 3) to discuss model errors in radiation and their impacts on energy budget, cloud type transition and circulation. Note that aerosol indirect effects are discussed in D4.4 and thus will not be included here. Also, for consistency, this report focuses on the region centred upon 5–10°N and 8°W–8°E. We shall refer to this region hereafter as the “DACCIWA region”.

2 Observations of cloud and aerosol radiative effects

This section documents work completed within the DACCIWA project, towards an improved understanding of how clouds and aerosols affect radiation budget over the DACCIWA region. Such an understanding is required to ultimately reduce persistent radiation errors found in atmospheric models in this region.

2.1 Cloud radiative effects

Radiative effects of various cloud types in the DACCIWA region are quantified using the state-of-the-art satellite datasets and radiative transfer. The *CERES–CloudSat–CALIPSO–MODIS* (CCCM) dataset (Kato et al., 2010; Kato et al., 2011; Ham et al., 2017), which combines observations from spaceborne active and passive instruments, provides detailed cloud profiles required for radiative transfer calculations. These cloud profiles were based on measurements of polar-orbiting satellites that cross the equator at approximately 0130 and 1330 local time (LT). The release B1 dataset is available from July 2006 to April 2011 inclusive. Since we focus on monsoon seasons in June–September to coincide with research activities of the DACCIWA project (Knippertz et al., 2015a; Hill et al., 2016; Hannak et al., 2017), the choice of the time period leads to a total data length of 19 months.

Radiative fluxes at the top of the atmosphere (TOA), at the surface, and heating rates in the atmosphere are calculated using the CCCM dataset as input to the Suite of Community Radiative Transfer Codes (SOCRATES) two-stream radiation scheme (Edwards & Slingo, 1996). The fluxes are evaluated against coincident the Clouds and the Earth's Radiant Energy System (CERES; Wielicki et al., 1996) measurements, showing good agreement with Pearson correlation coefficients of 0.95 for the TOA shortwave (SW) irradiances, 0.85 for the 1330 LT TOA longwave (LW) irradiances and 0.92 for the 0130 LT TOA LW irradiances. Diurnal mean irradiances in the LW are estimated by averaging the two CCCM sample times, while diurnal mean irradiances in the SW are estimated by running the calculations using 24 different solar zenith angles. More details can be found in Hill et al. (2018).

Following the scheme described in Tselioudis et al. (2013), each CCCM profile is classified as a cloud type based on its vertical structure. Pressure thresholds of 680 and 440 hPa are used to determine whether the profile contains one or more of low- (L), mid- (M), or high-level (H) cloud and whether cloud in different layers is connected or not. As illustrated in Fig. 1, this classification results in 13 different scene types, including clear sky and 12 cloud types.

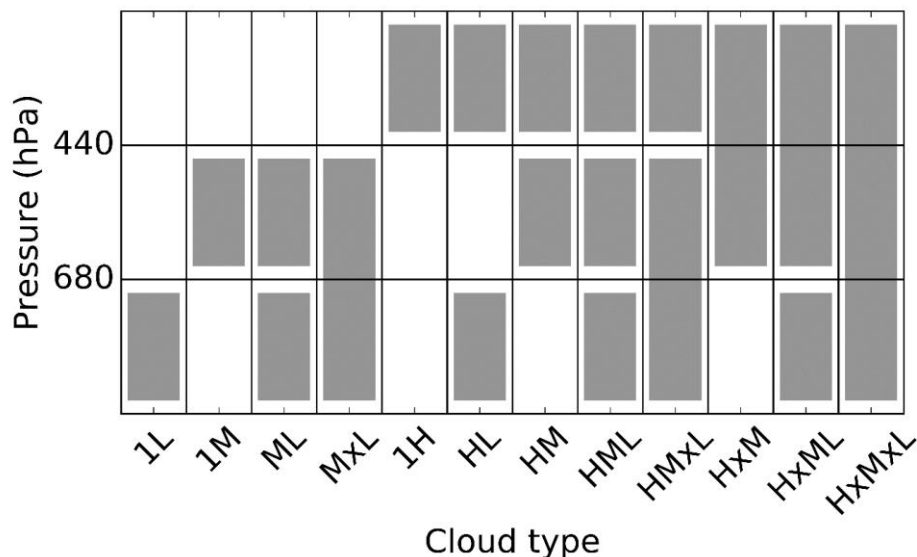


Fig. 1. Schematic illustrating how each cloudy CCCM profile is assigned to one of 12 cloud types based on the cloud vertical structure. L, M and H represent low-, mid- and high- clouds, respectively. Cloud occurring in multiple layers is denoted by a letter for each layer it occurs in, while the letter x is used to denote when cloud extends across the pressure boundaries. From Hill et al. (2018).

To provide further insight into how different cloud types affect the regional energy budget, the contribution to the total cloud radiative effect (CRE) from each cloud type is further decomposed into its frequency of occurrence and mean coincident cloud radiative effect (CCRE; i.e., the mean radiative effect calculated using only the CCCM group profiles that correspond to that cloud type). The frequency of occurrence of the different cloud types in Fig. 2 shows that the DACCIIWA region has infrequent clear sky and is very cloudy, in agreement with existing cloud climatology (Hill et al., 2016). The most common cloud types are 1L, 1H, and HL, but 8 of the 12 cloud types occur at least 5% of the time in this region, indicating a much more diverse set of cloud types than those found in many other parts of the globe (Tselioudis et al., 2013; Bodas-Salcedo et al., 2016). Multilayer clouds, where distinct clouds occur simultaneously in multiple layers, occur rather frequently (42% during the day and 46% during the night), representing a further source of complexity for understanding CRE.

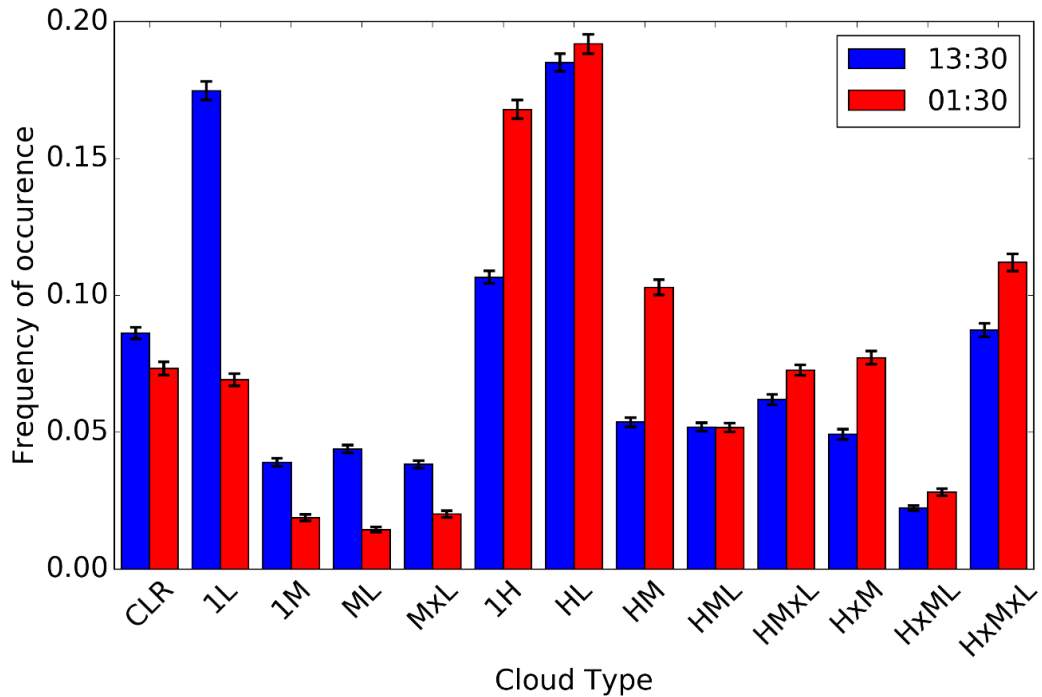


Fig. 2. Mean frequency of occurrence of each cloud type in the CCCM product over the DACCIIWA region in June–September, 2006–2010. Cloud frequency of occurrence at 1330 and 0130 LT are normalized separately. Uncertainty resulting from sampling is illustrated by the error bars, which show the 95% confidence interval based on bootstrapping. From Hill et al. (2018).

Over the DACCIIWA region, the CRE of different clouds depends on the particular irradiance in question (Hill et al., 2018). The CRE is complex, since almost all the cloud types make a non-negligible contribution to some aspect of the radiation budget. As shown in Fig. 3a, the mean SW CCRE of each cloud type at TOA is strongly linked to the number of layers it extends through, i.e., the physical thickness of cloud layers. This is not surprising, because physical thickness is correlated with water path and optical depth (Wang et al., 2000). The HxMxL cloud type, which extends into three layers and is likely to be deep convection, has the largest mean SW CCRE (476 W m^{-2} at 1330 LT). Those cloud types that extend between two layers have the next largest mean SW CCRE with values ranging from 275 to 297 W m^{-2} at 1330 LT. Clouds that occur separately in one or more layers have CCRE values ranging from 150 to 187 W m^{-2} at 1330 LT. The mean LW CCRE at TOA (Fig. 3b) is of a smaller magnitude compared to SW CCRE (Fig. 3a) for almost all cloud types, with isolated high cloud being the exception. Unlike SW, the magnitude of LW CCRE at TOA is mainly determined by cloud-top temperature, and thus closely linked to the presence of high cloud (e.g., 1H and HxMxL cloud types).

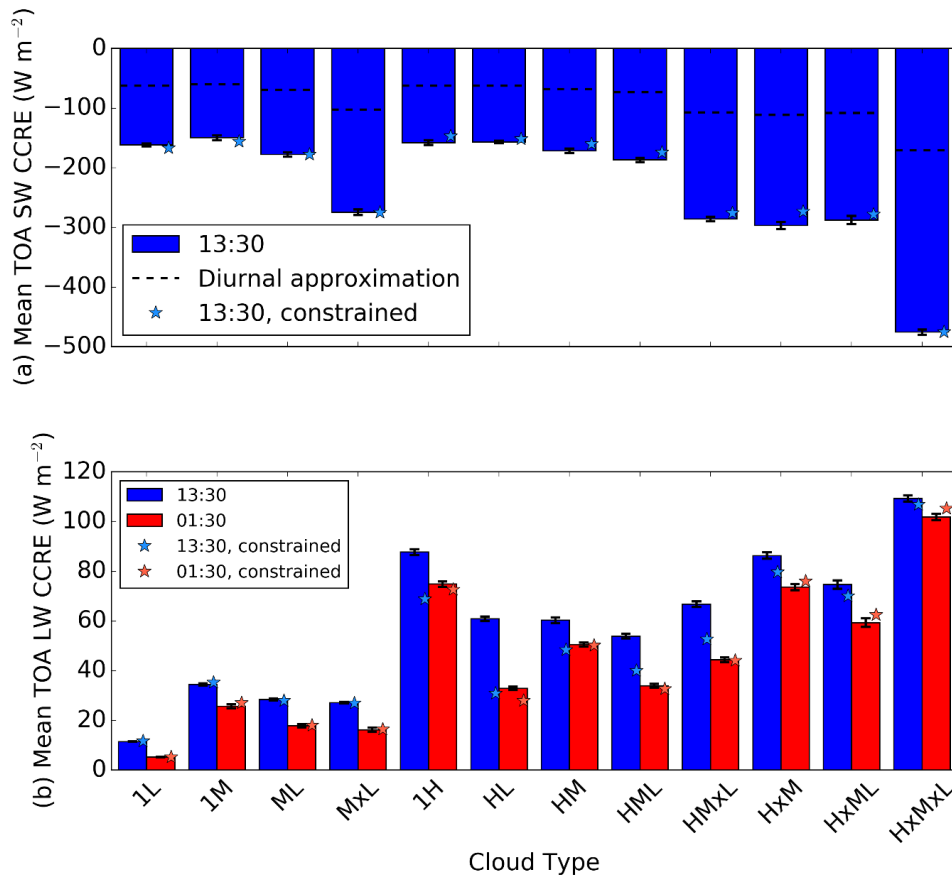


Fig. 3. The mean (a) SW and (b) LW mean CCRE at the TOA over the DACCIWA region over June–September, 2006–2010. Bars labelled 0130 and 1330 LT correspond to calculations based on the night-time and daytime satellite overpasses, respectively. The diurnal approximation shown in (a) is based on averaging calculations that use the daytime CCCM data and a range of solar zenith angles. Uncertainty resulting from errors in our calculations is illustrated by the constrained calculations, which exclude CCCM group profiles where the SOCRATES–CERES TOA differences are large. Error bars show the 95% confidence interval based on bootstrapping. From Hill et al. (2018)

Figure 4 shows the approximate diurnal mean total (i.e., SW + LW) cloud radiative effects. The diurnal mean total irradiances tend to be small because of cancellation between LW and SW CREs. For some cloud types, uncertainty is large (up to $\pm 7 \text{ W m}^{-2}$) at the TOA and surface, but the uncertainty is generally much smaller for fluxes into the atmosphere. At the TOA, the 1L cloud type has the largest magnitude net CRE, as the decrease in net downwelling SW irradiance resulting from low clouds is much larger than the increase in net downwelling LW irradiance. Most other cloud types also have a negative effect on the TOA net downwelling irradiance, although for many cloud types this is not certain. Isolated high cloud (1H) is the only cloud type that definitely leads to an increase in the net TOA irradiance. At the surface, all cloud types reduce the net downwelling irradiance, because the reduction in SW radiation reaching the surface is larger than the increase in downwelling LW radiation. 1L leads to a small reduction in the flux into the atmosphere, but all other cloud types increase the flux into the atmosphere.

For low clouds, a particular focus of the DACCIWA project, we have found that the 1L cloud type occurs with a frequency of 17 % at 1330 LT and 7 % at 0130 LT (Fig. 2). Low clouds that are beneath higher clouds occur more frequently, with a frequency of 31 % at 1330 LT and 29 % at

0130 LT. Note that these low clouds beneath higher clouds cannot easily be detected by passive satellite observations. Moreover, although these low clouds beneath higher clouds may not always have a particularly large effect on the TOA radiation budget, they do have a significant impact on the surface radiation budget (e.g. Fig. 9 in Hill et al. [2018]).

To summarize, the DACCIWA region experiences many different cloud types; no single cloud type dominates in terms of either frequency of occurrence or radiative effect. The most frequent cloud types are 1L, 1H, HL, and HxMxL, which have frequencies of 12%, 14%, 19%, and 10%, respectively. Contributions from different cloud types to the regional mean cloud radiative effect depend not only on their frequencies, but also on their mean CCRE, which is linked to cloud thickness in the SW and cloud-top and cloud-base height in the LW.

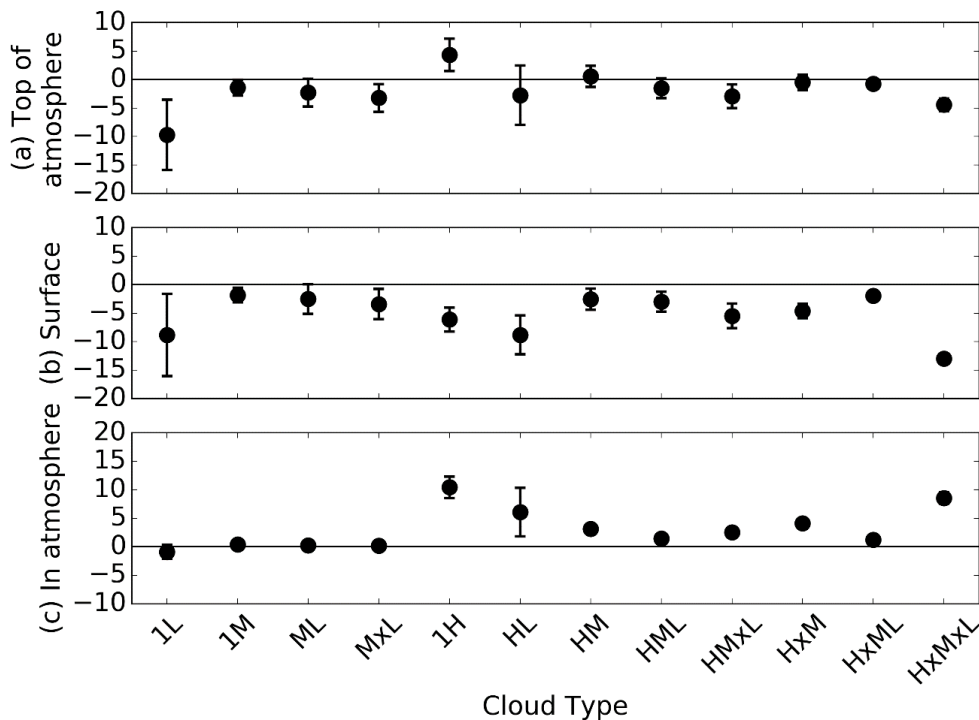


Fig. 4. Contribution to the diurnal mean total (i.e., SW + LW) CRE from each cloud type for June–September 2006–2010 over the DACCIWA region, based on radiative transfer calculations. Error bars show the combined uncertainty resulting from the diurnal mean approximation, the constrained calculation (which exclude CCCM group profiles where the SOCRATES–CERES TOA differences are large), and the limited sampling. These uncertainties are calculated separately for the SW and LW and are combined in quadrature. From Hill et al (2018).

2.2 Aerosol radiative effects

Similarly to cloud radiative effects, aerosol radiative effects are estimated by combining CCCM data with SOCRATES radiative transfer calculations. Seven common aerosol species are provided by CCCM, including soluble and insoluble particles, small and large dust particles, sulfuric acid, sea salt, and soot, as defined in the Optical Properties of Aerosols and Clouds (OPAC) climatology (Hess et al., 1998). The extinction CCCM attributes to each species depends on CALIPSO measurements and the Model of Atmospheric Transport and Chemistry (MATCH; Rasch et al., 1997). The extinction, single scattering albedo, and asymmetry of these aerosol species are spectrally dependent and parameterized in SOCRATES as a function of aerosol mass mixing ratio, as described in Cusack et al. (1998). Since the CCCM dataset does not provide mass mixing ratio

directly, we used the inverse of the SOCRATES parameterization to derive profiles of aerosol mass mixing ratios from the CCCM aerosol extinction profiles for each species. These aerosol mass mixing profiles are then input to SOCRATES for radiative transfer calculations. Additionally, the diurnal means of radiative effects at TOA are estimated by averaging LW irradiances at 1330 and 0130 LT for the LW, and by multiplying the SW irradiances at 1330 LT by a factor of 0.396 for the SW. This multiplying factor was estimated by comparing the SW irradiances at 1330 LT to the mean of the hourly SW irradiances at TOA.

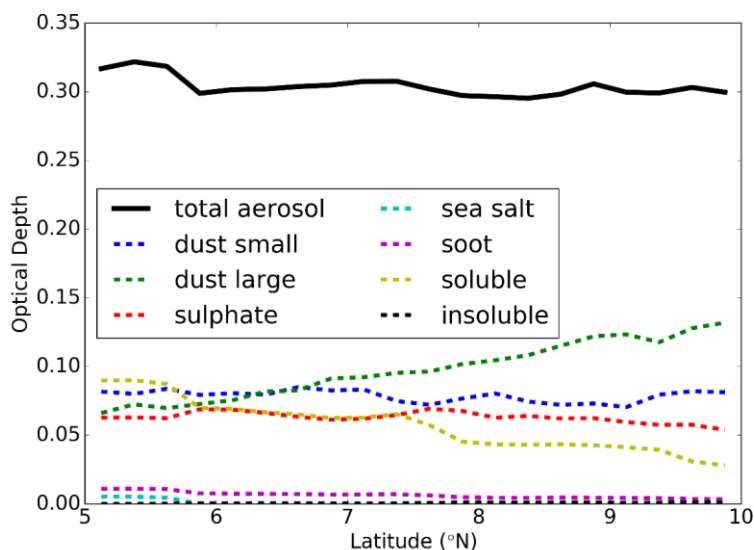


Fig. 5. Zonal mean aerosol optical depth at 500 nm for the DACCIIWA region, from the CCCM dataset for June–September, 2006–2010. The solid black line indicates the total aerosol optical depth from all aerosol species, while each of the broken lines indicates the optical depth due to one of the seven aerosol species included in CCCM.

Figure 5 shows the zonal mean aerosol optical depth attributed to each species in CCCM. The total aerosol optical depth is ~ 0.32 near the coast and decreases to ~ 0.3 inland. This value of 0.3 generally agrees with the mean AOD measured by the NASA Aerosol Robotic Network (AERONET) in June–July 2016, as described by Mollard et al. (2018). Although the total optical depth is rather constant, individual aerosol species show different variability with latitude. The optical depth of small dust aerosols remains fairly constant with latitude, but the optical depth of large dust particles increases with latitude, as distance to the major dust source decreases. The sulphate aerosol corresponds to stratospheric background aerosol and thus it is unsurprising that its optical depth shows little variation with latitude. Extinction due to sea salt is negligible at most latitudes, with larger (but still small) optical depth at the coast. The optical depth of soot is also very small, with largest values again at the coast. Soluble aerosol corresponds to pollution and as a result the optical depth is largest near the coast where the large cities (i.e., the main emission sources) are located and decreases with latitude. Finally, the optical depth of insoluble aerosols, which correspond to soil particles, is negligible at all latitudes. Since DACCIIWA aircraft measurements show that the regional pollution is dominated by biomass burning (Haslett et al., in preparation), the CCCM product might have underestimated the optical depth of soot.

The zonal mean direct aerosol radiative effect (DARE) for both the SW and LW at both TOA and surface is shown in Fig. 6. Similar to CRE, the DARE is defined as the difference of irradiances computed with and without aerosols. Since aerosol radiative effects are influenced by the

associated cloud conditions, we show separate estimates of the aerosol radiative effects using both all-sky (i.e. including the observed cloud) and clear-sky (i.e. removing all cloud) calculations.

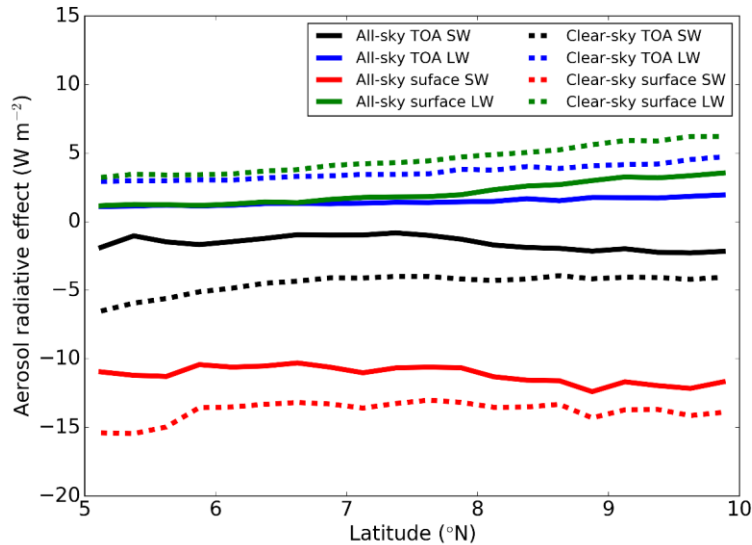


Fig. 6. Zonal mean aerosol direct radiative effects for the DACCIWA region in June–September 2006–2010, based on CCCM data and SOCRATES calculations with and without aerosols. “All-sky” values (solid lines) are computed including clouds in radiative transfer, while “clear-sky” values (broken lines) are computed excluding clouds in radiative transfer calculations with and without aerosols.

Beginning with the LW, we see that aerosols lead to an increase in the net downwelling LW irradiance at both the surface and TOA. All-sky DARE increases from $\sim 1 \text{ W m}^{-2}$ near the coast to ~ 2 and $\sim 4 \text{ W m}^{-2}$ near 10°N at the TOA and surface, respectively. If clouds are excluded from the calculations (i.e., clear-sky estimates), LW DARE are consistently $\sim 3 \text{ W m}^{-2}$ larger at both the TOA and surface for all latitudes, remaining the increase.

The increase with latitude in LW DARE is thought to be due to the changes in aerosol species. Recall that Fig. 5 presents optical depth at 500 nm , a wavelength in the SW. Let us focus on two aerosol species in Fig. 5: one is large dust particles that show the largest increase in optical depth with latitude, and the second is soluble particles that show the largest decrease in optical depth with latitude. The opposite changes with altitude in these two species help maintain the total optical depth at 500 nm to be nearly constant. However, the extinction per unit mass of soluble particles in the LW is at least 10 times smaller than that at 500 nm , while the extinction per unit mass of large dust particles in the LW is similar to that at 500 nm . As a result, in the LW, the increase in extinction with latitude due to increased concentrations of large dust particles is larger than the decrease in extinction due to decreased concentrations of soluble particles. This leads to an increase in the total extinction in the LW increases with latitude, and the increase LW DARE with latitude seen in Fig. 6.

In the SW, aerosols lead to a decrease in the net downwelling SW irradiance at both the surface and TOA. At the surface, the clear-sky DARE is approximately -15 W m^{-2} near the coast and decreases to about -13.5 W m^{-2} at higher latitudes. This is a direct consequence of the changes in the total aerosol optical depth with latitude. At the TOA, the DARE is smaller than at the surface, as absorption by aerosols reduces the amount of downwelling SW irradiance, but does not necessarily change the upwelling SW irradiance. The magnitude of the clear-sky SW DARE at

TOA decreases with latitude between the coast and $\sim 7^\circ\text{N}$. This is due to an increase in absorption by aerosols as the concentrations of more scattering aerosols (e.g. soluble) decrease with latitude, while the concentrations of more absorbing aerosols (e.g. large dust) increase with latitude, as shown in Fig. 5. The all-sky surface SW DARE is smaller in magnitude, as clouds extinguish some of the radiation that is extinguished by aerosols in the clear-sky case.

Although both the mean AOD and mean SW incoming irradiance used in our calculations are larger than the global averages, the zonal mean calculated clear-sky values for the SW DARE at TOA are similar to estimates of the global mean over land at both the TOA (between -1.7 and -5.5 W m^{-2}) and surface (between -5.1 and -13.5 W m^{-2}) as estimated by Yu et al. (2006). Our calculated zonal mean is also very close to the value of 5.82 W m^{-2} estimated by Mollard et al. (2018) using AERONET aerosol properties and assuming clear-sky at Save (note the difference in sign is due to comparing the DARE on net downwelling TOA SW irradiances to the DARE for upwelling TOA SW irradiances). However, the SW surface DARE is notably $\sim 10 \text{ W m}^{-2}$ smaller in magnitude than the value of -26.08 W m^{-2} calculated by Mollard et al. (2018). About 5 W m^{-2} of this difference is because the results presented here are net downwelling (i.e. down-up) as opposed to downwelling. Since the TOA DARE values are in good agreement, the other 5 W m^{-2} difference must be due to additional atmospheric absorption from aerosols in the AERONET calculations.

3 Evaluation of model radiation

3.1 DACCIWA campaign forecasts

As part of the forecast evaluation reported in D7.3, several model forecasts were verified using Outgoing Longwave Radiation (OLR) using measurements from Geostationary Earth Radiation Budget (GERB) instrument processed at the University of Reading.

GERB is the geostationary earth radiation budget instrument onboard the EUMETSAT's Meteosat Second Generation (MSG) satellites (Harries et al., 2005). It is a broadband radiometer designed to measure the total emitted and solar reflected radiances over the earth with high temporal resolution (5 min) and 50 km spatial resolution. From the measurements, the top of atmosphere radiation, divided in short and longwave contributions can be estimated to give an accurate estimation of the earth's radiation budget (or rather the budget in MSG's field of view which covers almost half of the earth's surface).

GERB measurements were averaged of the preceding three hours, calculated from measurements every 15 minutes. To avoid biasing the fluxes due to diurnal sampling, if any GERB data in the three-hour window was missing, the three-hour average was set to missing. GERB solar flux suffers from sun-glint over water surfaces at low zenith angles, which means that these are often missing. Note that when sun glint occurs, the daily means are biased low because it occurs at low zenith angles. GERB solar flux is only measured for zenith angles less than 80° . The data were extended to 104.5° using CERES twilight measurements and interpolation as described in Hill et al. (2016).

Figure 7 shows OLR time series and errors for the pre-onset and post-onset periods, as defined by Knippertz et al. (2017). Most forecast models have a lower bias in the post-onset period than in the pre-onset but large centred root mean square error (CRMSE) in both periods. A small exception is the COSMO model that displays a large bias in the post-onset period, possibly connected with an underestimation of cirrus outflow resulting from deep convection.

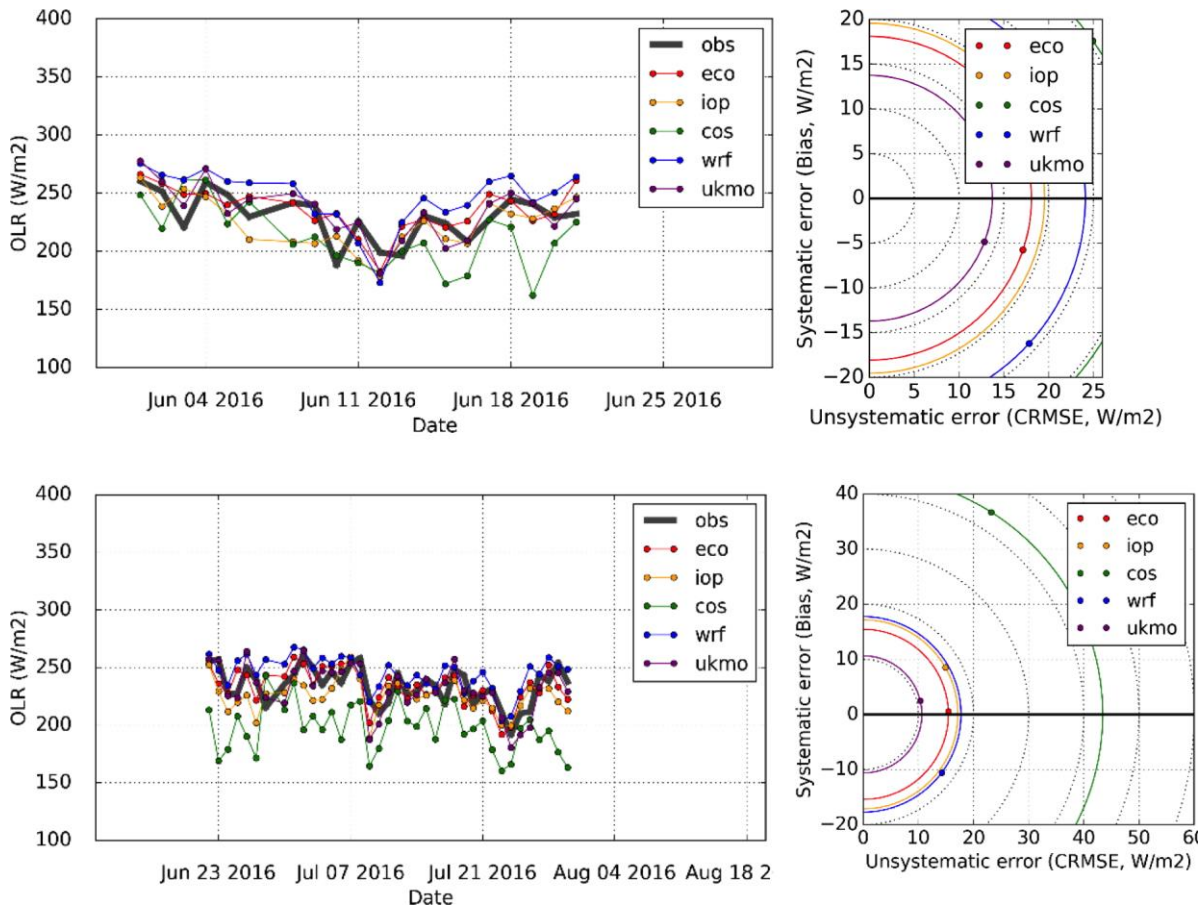


Fig. 7. Box-average OLR from the various models compared with GERB observations during the DACCIWA campaign. Left: Time-series. Right: Error diagrams with contributions from systematic and unsystematic errors to the Root Mean Square Error with the different times of day combined. The latter is referred to as “centred root mean square error (CRMSE)”. Top: pre-onset period; Bottom: post-onset period. (From Fig. 13, D7.3.)

3.2 Global atmospheric models

A detailed evaluation of the DACCIWA climate models was presented in D7.4. We present results from an evaluation of the representation of the West African monsoon (WAM) system in widely used global and regional climate and seasonal model datasets following a similar strategy as in D7.3 for weather forecasting. Here we present a sub-set of D7.4 focusing on TOA radiative fields. Considered model datasets include (a) long-term climate simulations from the Coupled Model Intercomparison Project Phase 5 (CMIP5) coordinated by the Intergovernmental Panel on Climate Change (IPCC), (b) climate simulations conducted as part of the Years of Tropical Convection (YoTC; Waliser et al., 2012), which provides additional tendency terms and diurnally resolved data, (c) own climate simulations using the ECHAM6 (run by ETHZ) and Unified Model (run by MO), and (d) seasonal forecasts using the ECMWF Integrated Forecast System (IFS). Outgoing longwave and shortwave radiation from forecast models were evaluated against GERB products. We used the “Standard High-resolution Image” (Dewitte et al., 2008), in which the data are processed using cloud observations from SEVIRI to convert radiance measurements to radiative fluxes at approximately 10 km resolution, every 15 min.

As shown in Fig. 8, the highest values of OLR from GERB are found in the southern west corner of the DACCIWA box, the smallest ones in the southern right corner, while a triangle-shaped region with medium values can be found in between. This pattern is very well repeated by the IFS runs,

and most other models show at least the maximum in approximately the right position. The absolute values are too high from all models but IFS. Hence, the radiative effect of clouds is not modelled in the right way. The GERB outgoing shortwave radiation (OSR) field places the smallest values at the southern edge in the centre with larger values shortly northwards from it. All models show the same structure but the absolute values vary in a range of 190 W m^{-2} which is much more than for OLR (55 W m^{-2}).

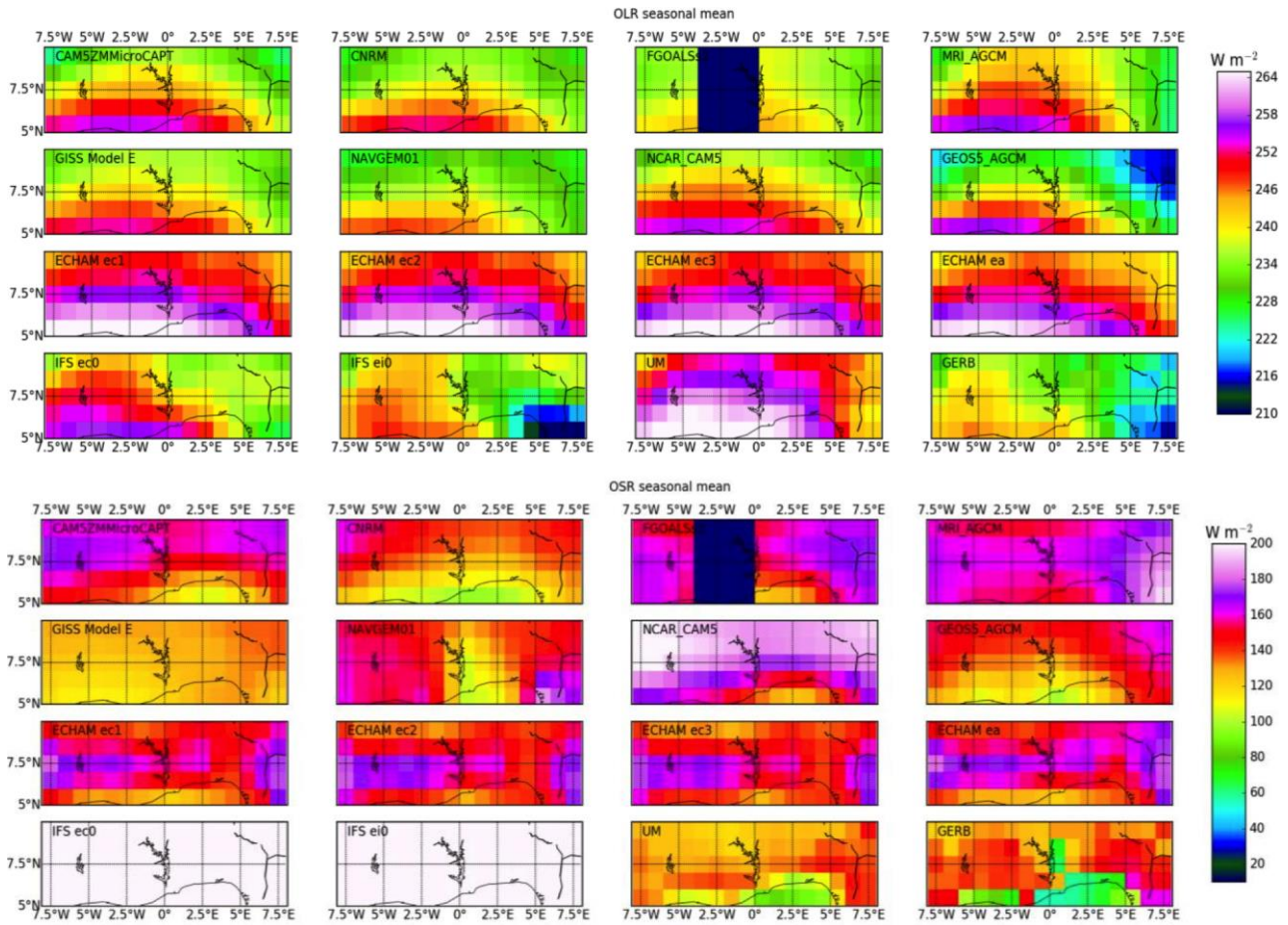


Fig. 8. Outgoing longwave radiation (upper panel) and outgoing shortwave radiation (lower panel) at top of the atmosphere as seasonal mean for the YOTC models, the ECHAM and the IFS runs and the UM compared to GERB measurements from 2006–2015. Please note that for IFS only net radiation was available, therefore shortwave fields cannot be shown and for the longwave fields the incoming longwave radiation was assumed to be exactly zero.

The influence of clouds on outgoing shortwave and longwave radiation varies from model to model. The UM had by far the lowest amount of liquid water and not too much ice water, therefore it is not surprising that the seasonal mean of OLR for the UM is largest compared to the other models. For the other models the effect of clouds is not easy to describe without additional information, e.g. NAVGEM does not have a lot of liquid water or ice but at the same time not a very high OLR. This could either mean that the diurnal cycle is very strong and no general conclusions can be drawn from comparing a figure for 12 UTC with all-day averages, or that the microphysical properties of the clouds contribute strongly to the observed variation.

3.3 Further analysis of climate models

Having examined radiation errors in models, this section examines TOA irradiances in greater detail in climate models. In particular, we analyse interannual variability and diurnal cycles in the climate models and identify the causes of errors in these models by considering all-sky and clear-sky irradiances separately. Further details concerning this analysis are available from Hill et al (2016).

We base this analysis on simulations from CMIP5 (Taylor et al., 2012). As this study is focused on atmospheric processes, we use Atmospheric Model Intercomparison Project (AMIP) simulations that employ predetermined realistic sea surface temperatures and sea ice. Additionally, since the DACCIWA region exhibits notable diurnal cycles of cloud and hence radiation (Stein et al., 2011; van der Linden et al., 2015), we also focus on those AMIP5 models for which 3-hourly output is available: CanAM4, CNRM-CM5, HadGEM2-A, and MRI-CGCM3. We focus on the months of June and July, using 1) data from 2008 for which 3 hourly model output is available for diurnal cycle comparisons, and 2) all available years from 2002 onwards for diurnal mean comparisons.

We use the CERES data set to evaluate these climate models. CERES instruments are limited to two polar-orbiting satellites and as a result only sample four points in the diurnal cycle. The CERES instrument on the AQUA satellite takes radiation measurements over the DACCIWA region at approximately 0130 and 1330 LT, while the CERES instrument on board the TERRA satellite takes measurements over the DACCIWA region at approximately 1030 and 2230 LT. To obtain better sampling of the diurnal cycle, we use the synoptic radiative fluxes and clouds (CERES-SYN) product (Doelling et al., 2013), which capitalizes on geostationary imagers to estimate the diurnal variability between CERES observations. For consistency with the climate models, we use CERES-SYN data from June–July 2008 for diurnal cycle comparisons and June–July 2002–2014 for diurnal mean comparisons.

Figure 9 shows the June–July mean all-sky and clear-sky irradiances for the CERES-SYN product and the four AMIP models. For the TOA SW irradiances, interannual variability in each of the models is large. The interannual variability in the CERES-SYN product is smaller. Two of the AMIP models consistently overestimate the TOA outgoing SW irradiance compared to CERES-SYN, while two underestimate it. For TOA LW irradiances, the modelled interannual variability is again larger than the observed interannual variability. Generally the climate models overestimate the TOA outgoing LW irradiance, but only one of the climate models (HadGEM2-A) overestimates the TOA outgoing LW irradiance by a significant amount.

Examining clear-sky irradiances can help determine whether the all-sky irradiance errors are due to cloud or other processes such as aerosols, water vapour, or the surface albedo. However, it is important to bear in mind that the models and satellite observations determine clear-sky irradiances quite differently. In the models, clear-sky irradiances are calculated by repeating radiative transfer calculations without cloud. In the observations, clear-sky irradiances are estimated by averaging the measurements for pixels that are identified as cloud free. This can lead to differences in mean clear-sky irradiances as large as 15 W m^{-2} in the LW (Allan and Ringer, 2003). Nevertheless, this difference is apparently much smaller than the model bias shown in Fig. 9. For SW, there is a clear climate model bias in clear-sky conditions: all four AMIP models have larger irradiances than CERES-SYN. In particular, the clear-sky bias in the MRI-CGCM3 model can explain most of the all-sky bias. Hill et al. (2016) found that this is primarily because MRI-CGCM3 has a much larger surface albedo than the other models, highlighting the need for improved observational surface albedo datasets in this region. For the HadGEM2-A and CNRM-CM5 models, the clear-sky bias appears to partially offset cloud errors and reduce all-sky

TOA SW irradiance errors. LW clear-sky errors diurnal mean errors are much smaller and we cannot identify any definite biases given the uncertainty related to different definitions of clear-sky.

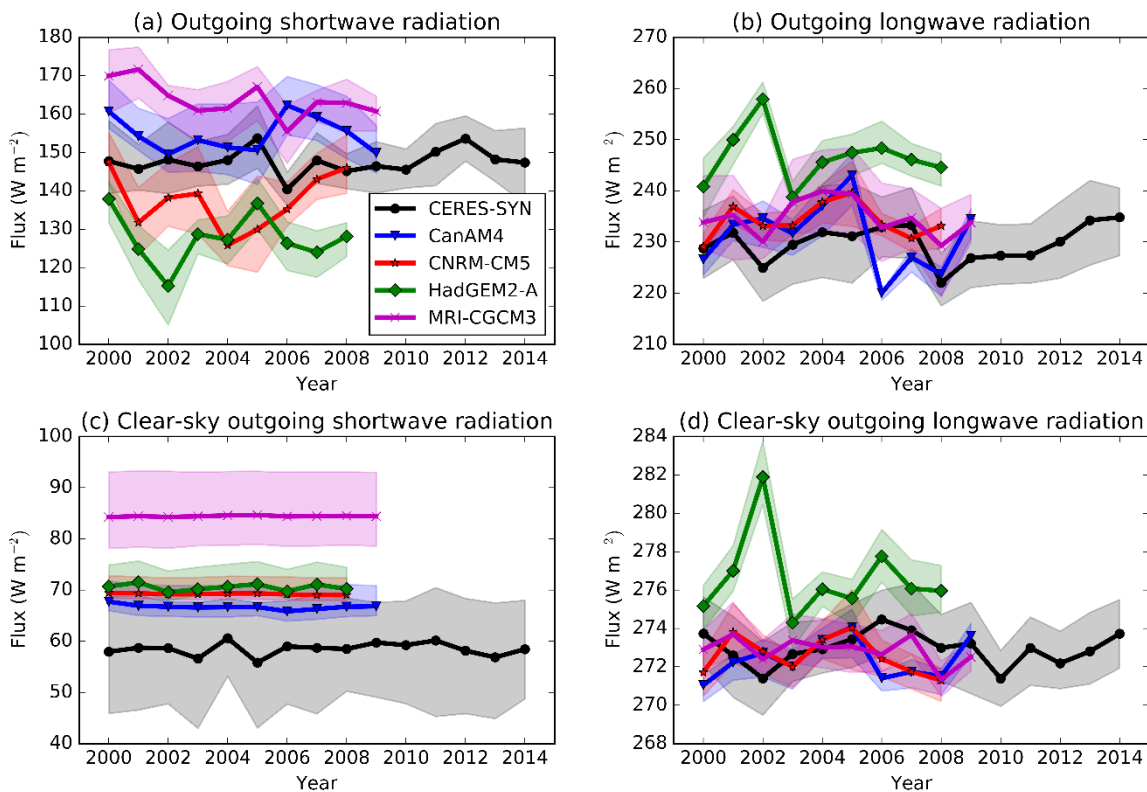


Fig. 9. June-July mean top of atmosphere radiative fluxes in the DACCIWA region for CERES-SYN and AMIP5 models. Shading shows spatial variability within the domain. Adapted from Hill et al. (2016).

Figure 10 compares diurnal cycle of TOA irradiances from the models and CERES-SYN. Differences in the phase of the diurnal cycles of irradiances cannot be disentangled from the temporal sampling that the climate models use to reduce the cost of the computationally expensive radiative transfer schemes. The different climate models use different methods to account for this reduced temporal sampling, and as a result irradiances output at the same point in time may represent quite different time periods. Such differences make comparison of the phase of the diurnal cycles of radiation problematic, so we shall restrict our discussion to the amplitude of the diurnal cycles.

For SW irradiances, the amplitude of the diurnal cycle is dominated by changes in the solar zenith angle. Differences in the amplitudes of the SW diurnal cycles are consistent with differences in diurnal mean irradiances. For LW clear-sky irradiances at TOA, all the models have a larger amplitude diurnal cycle than CERES-SYN. This may be due to the different methods for calculating clear-sky irradiances. However, two of the climate models (HadGEM2-A and CanAM4) have significantly larger amplitude all-sky diurnal cycles than CERES-SYN, which implies there are issues with the diurnal cycles of cloud in these models.

OLR is generally overestimated in the climate models shown in Figs. 8–10. Further analysis of some of the climate models shows that the clear-sky OLR predicted by these models is much closer to the observed values than the all-sky OLR, which points to problems simulating the radiative effect of high clouds in this region. Many (but not all) of the models also overestimate the OSR compared to satellite observations, but analysis of clear-sky OSR in some of the models

reveals large differences amongst models and between the models and the satellite observations, which may be able to explain large parts of the all-sky errors.

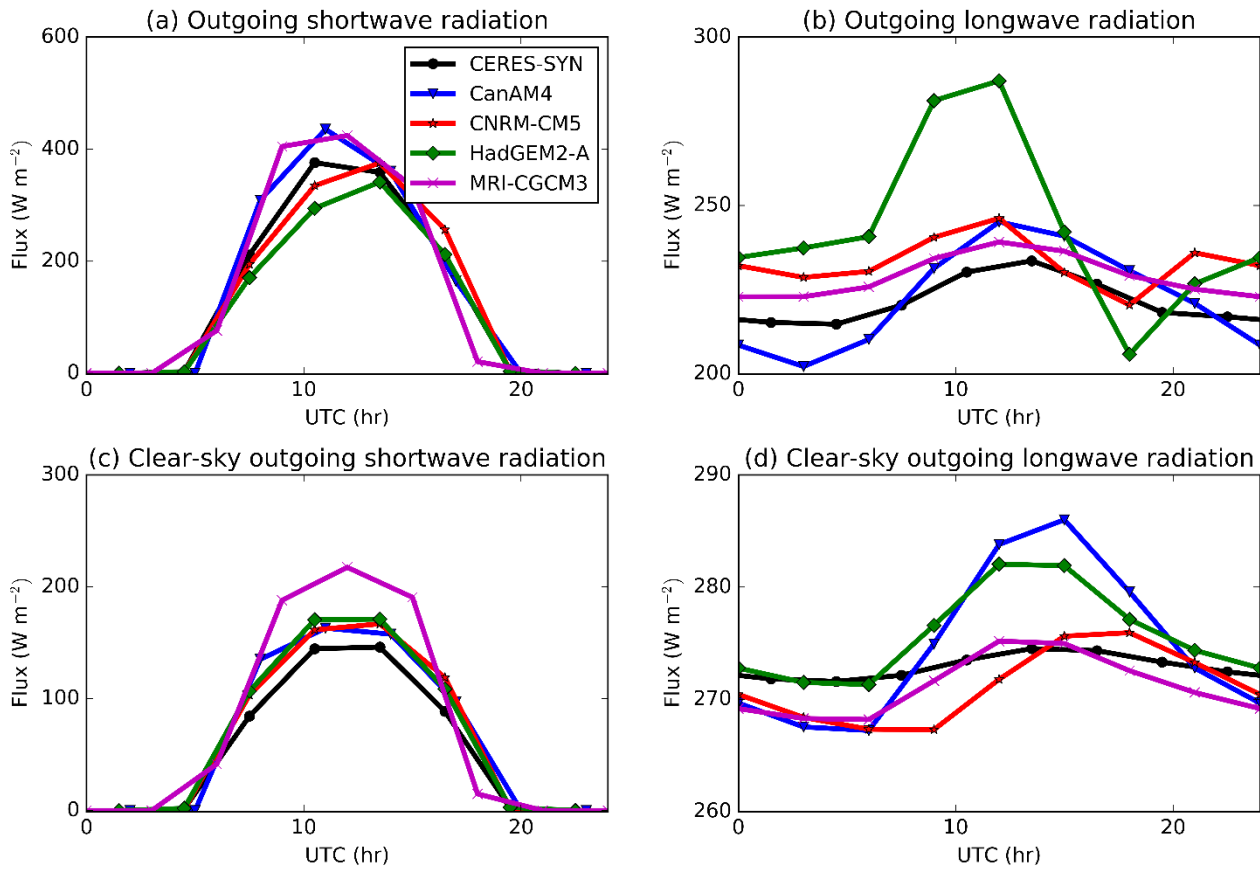


Fig. 10. Comparison of diurnal cycles for June–July 2008. For shortwave radiation (a and c), the models are shown at a time that is most consistent with the solar zenith angle used, rather than the output time. From Hill et al. (2016).

4 Effect of radiative processes on circulation

Radiation errors are of interest because errors in radiative heating cause further errors in circulation and precipitation. This section aims to identify potential consequences of the model radiation errors identified in the previous section.

4.1 Energy budget analysis

One of the simplest methods for understanding how radiation is linked to circulation and precipitation is to construct energy budgets. Under the hydrostatic approximation and assuming that kinetic energy transport and changes in energy and water storage are negligible as in Muller and O’Gorman (2011), the time-mean regional atmospheric energy budget may be expressed as

$$L_c P = Q + H_d$$

where L_c is the latent heat of condensation of water vapor, P is the surface precipitation rate, H_d is the atmospheric horizontal divergence of dry static energy and Q is the atmospheric net heating from radiation and sensible heat.

Satellite datasets provide estimates of precipitation rates, SW column radiative heating and LW column radiative cooling, while we take estimates of sensible heating, surface evaporation,

divergence of moisture and divergence of dry static energy from the ERA-Interim reanalysis (Dee et al., 2011). Figure 11 illustrates the atmospheric energy budget of the DACCIWA region, including June–July multi-annual mean estimates for each term. The DACCIWA region is fueled by a combination of $\sim 110 \text{ W m}^{-2}$ of SW radiative heating, $\sim 170 \text{ W m}^{-2}$ of latent energy, and $\sim 25 \text{ W m}^{-2}$ of sensible heating from the surface. This is balanced by LW net radiative cooling between -188 and -211 W m^{-2} (depending on dataset) and horizontal divergence of dry static energy of approximately -105 W m^{-2} .

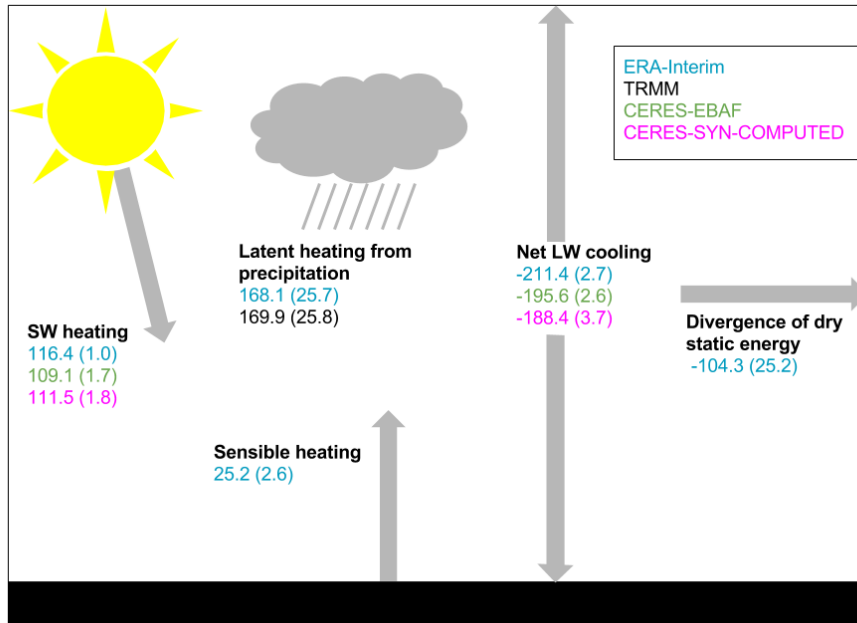


Fig. 11. Key terms in the atmospheric energy budget for the DACCIWA region. Numbers shown are June–July means (standard deviations of interannual means in parentheses) for 2000–2015 from the data source indicated by that colour. From Hill et al. (2016).

4.2 Effect of SW irradiance perturbations on regional precipitation and circulation

Deetz et al. (2018) investigate the total (direct + indirect) aerosol effect using COSMO-ART simulations. By scaling aerosol concentrations within their simulations, they found that increasing aerosol concentrations led to decreased surface downwelling SW irradiance, due primarily to the aerosol direct effect. This in turn affects two features of the regional meteorology: the stratus to cumulus transition (SCT) that takes place in the DACCIWA region in the course of the day, and the Atlantic (or maritime) Inflow – a coastal front that develops during daytime and propagates inland during the evening.

The reduction in downwelling surface SW irradiance affects the SCT through decreased surface temperatures, which in turn lead to decreased sensible heat fluxes. This in turn reduces the boundary layer height and consequently the cloud base height, leading to an later break-up of the stratus cloud. The effect of the reduction in surface SW irradiance on the Atlantic Inflow is also through decreased surface temperature. This reduction in surface temperature leads to increased surface pressure, which leads to a decrease in the Atlantic Inflow front velocity.

Additionally, Kniffka et al. (2018) examine how the radiative effect of low-level clouds affects the regional meteorology, using a regional numerical weather prediction model. They ran simulations with the Icosahedral Nonhydrostatic (ICON) model over the DACCIWA region and analysed the

effect of changing the condensed water content below 700 hPa passed to the radiation scheme used by their model. In contrast to Deetz et al. (2018), they found significant impacts on the regional precipitation, with decreasing surface precipitation as the low cloud water content increased. They argued that this was because increasing low cloud water content leads to decreased surface SW irradiance, which leads to decreased surface temperature and a more stable boundary layer, leading to less triggering of convection. They also found large effects on the diurnal cycle of clouds in the region. However, the changes in low cloud water content had little impact outside the DACCIWA region in which they were applied.

Both these studies illustrate the sensitivity of the regional meteorology to the radiative processes. Moreover, although the radiative perturbations in both studies are similar (i.e. primarily changing the downwelling SW irradiance at the surface), the model responses are quite different. These two different studies perturbed the radiation budget using different methods, resulting in different perturbations, and were run for different time periods. Thus, it is unclear whether the differing model responses are due to differences in the radiative perturbations, differences in the regional meteorology, differences in the way the models respond to these perturbations, or a combination of all three. These are just two studies using only two models. It remains to be seen whether these results can be confirmed in observations and/or generalised to other models. It would also be very useful to analyse these simulations within the context of the regional energy budget.

5 Summary and conclusions

This report addresses specific objectives that Work Package 5 set out to achieve, namely quantifying the impacts of low and mid-level clouds (layered and deeper congestus) and aerosols on the energy budget, evaluating and improving state-of-the-art satellite cloud/aerosol retrievals and models, and analyzing the effect of cloud radiative forcing on the West Africa monsoon circulation.

We have found that low clouds that are beneath higher clouds occur frequently, approximately 30% both at daytime and nighttime. In contrast, single-layer low clouds occur much less frequently and appear to have a more evident daytime (17%) and nighttime (7%) difference. Similar to other types of clouds, single-layer low cloud has a moderate negative radiative effect at TOA in the SW and a small positive effect in the LW. Due to the compensation between SW and LW, the diurnal mean of the total radiative effect of single-layer low clouds is about -10 W m^{-2} both at TOA and at the surface. The magnitude of the low-cloud radiative effect is the largest compared to other cloud types (except the radiative effects of deep convective clouds at the surface) and is associated with the largest uncertainty, highlighting the importance of continuous capability for better cloud observations.

Similarly to clouds, aerosols have a negative direct radiative effect in the SW and a positive effect in the LW in both all-sky and clear-sky conditions. The total direct effect of aerosol is in the order of -10 W m^{-2} . The aerosol direct radiative effect does not show a strong variation in latitude; however, the lack of strong zonal variation is because the effects from different aerosol species compensate each other, due to changes in aerosol concentration with latitude and due to the difference in their absorption properties. While our estimates from satellite retrievals generally agree with those estimated from a global scale, there is a non-negligible discrepancy between our estimates and those from field campaign data. This discrepancy suggests that better observations of aerosol absorption properties may be the key element for reducing the uncertainty in aerosol direct radiative effects.

Focusing on outgoing radiative fluxes, models continue to show large biases in both SW and LW, and larger interannual variability compared to the state-of-the-art satellite observations. While these persistent errors are highly linked to the ability to model clouds, our analysis shows that calculations in clear-sky conditions also require caution and improvement, but the sources of errors tend to be more easily identified compared to all-sky conditions.

The effect of SW irradiance on regional precipitation and circulation are investigated through model simulations. The SW irradiance is perturbed through increased aerosol concentration and low-level cloud water amount, leading to different model response. Studies from the DACCIIWA partners demonstrate that model responses can include delayed stratocumulus-to-cumulus transition, reduced marine flow, more stable boundary layer and reduced convection activity. Since these responses can be diverse and sensitive to the details of model schemes and setup, more efforts on the modeling and observational constraints will be needed to confirm how robust these responses are.

6 References

Allan, R. P. and Ringer, M., 2003. Inconsistencies between satellite estimates of longwave cloud forcing and dynamical fields from reanalyses. *Geophys. Res. Lett.*, 30(1491).

Bodas-Salcedo, A. et al., 2016. Large Contribution of Supercooled Liquid Clouds to the Solar Radiation Budget of the Southern Ocean. *Journal of Climate*, 29(11), pp. 4213-4228.

Cusack, S., Slingo, A., Edwards, J. M. & Wild, M., 1998. The radiative impact of a simple aerosol climatology on the Hadley Centre atmospheric GCM. *Q.J.R. Meteorol. Soc.*, 124(551), pp. 2517-2526.

Dee, D. P. et al., 2011. The ERA-Interim reanalysis: configuration and performance of the data assimilation system. *Q.J.R. Meteorol. Soc.*, 137(656), pp. 553-597.

Deetz, K. et al., 2018. Numerical simulations of aerosol radiative effects and their impact on clouds and atmospheric dynamics over southern West Africa. *Atmos. Chem. Phys.*, Volume 18, pp. 9767-9788.

Dewitte, S. et al., 2008. The Geostationary Earth Radiation Budget Edition 1 data processing algorithms. *Advances in Space Research*, 41(11), pp. 1906-1913.

Doelling, D. R. et al., 2013. Geostationary Enhanced Temporal Interpolation for CERES Flux Products. *J. Atmos. Oceanic Technol.*, 30(6), pp. 1072-1090.

Edwards, J. M. & Slingo, A., 1996. Studies with a flexible new radiation code. I: Choosing a configuration for a large-scale model. *Q.J.R. Meteorol. Soc.*, 122(531), p. 689–719.

Ham, S.-H. et al., 2017. Cloud occurrences and cloud radiative effects (CREs) from CERES-CALIPSO-CloudSat-MODIS (CCCM) and CloudSat radar-lidar (RL) products. *J. Geophys. Res. Atmos.*, 122(16), pp. 8852-8884.

Hannak, L. et al., 2017. Why Do Global Climate Models Struggle to Represent Low-Level Clouds in the West African Summer Monsoon?. *Journal of Climate*, 30(5), pp. 1665-1687.

Harries, J. E. et al., 2005. The Geostationary Earth Radiation Budget Project. *Bull. Amer. Meteor. Soc.*, 86(7), pp. 945-960.

- Hess, M., Koepke, P. & Schult, I., 1998. Optical Properties of Aerosols and Clouds: The Software Package OPAC. *Bull. Amer. Meteor. Soc.*, Volume 79, pp. 831-844.
- Hill, P. G. et al., 2018. Quantifying the Contribution of Different Cloud Types to the Radiation Budget in Southern West Africa. *J. Climate*, Volume 31, pp. 5273-5291.
- Hill, P. G., Allan, R. P., Chiu, J. C. & Stein, T. H. M., 2016. A multi-satellite climatology of clouds, radiation and precipitation in southern West Africa and comparison to climate models. *J. Geophys. Res. Atmos.*, 121(18), pp. 10,857-10,879.
- Kato, S. et al., 2011. Improvements of top-of-atmosphere and surface irradiance computations with CALIPSO-, CloudSat-, and MODIS-derived cloud and aerosol properties. *J. Geophys. Res. Atmos.*, 116(D19).
- Kato, S. et al., 2010. Relationships among cloud occurrence frequency, overlap and effective thickness derived from CALIPSO and CloudSat merged vertical profiles. *J. Geophys. Res. Atmos.*, 115(D00H28).
- Kniffka, A., Knippertz, P. & Fink, A. H., 2018. The role of low-level clouds in the West African monsoon system. *Atmos. Chem. Phys. Discuss.*, in review.
- Knippertz, P. et al., 2015a. The DACCIWA Project: Dynamics–Aerosol–Chemistry–Cloud Interactions in West Africa.. *Bull. Amer. Meteor. Soc.*, Volume 96, pp. 1451-1460.
- Knippertz, P. et al., 2015b. The possible role of local air pollution in climate change in West Africa. *Nat. Climate Change*, Volume 5, pp. 815-822.
- Knippertz, P. et al., 2017. A meteorological and chemical overview of the DACCIWA field campaign in West Africa in June–July 2016. *Atmos. Chem. Phys.*, Volume 17, pp. 10893-10918.
- Loeb, N., 2008. *CERES Level 2 NEWS CCCM Aqua-FM3-MODIS-CAL-CS HDF File - Release B1 [Data set]*. s.l.:NASA Langley Atmospheric Science Data Center DAAC.
- Mollard, J. D. P. et al., 2018. An assessment of satellite aerosol products in Western Africa during the Monsoon using DACCIWA observations. *In prep.*.
- Muller, C. J. & O'Gorman, P. A., 2011. An energetic perspective on the regional response of precipitation to climate change. *Nature Climate Change*, 1(5), pp. 266-271.
- Rasch, P. J., Mahowald, N. M. & Eaton, B., 1997. Representations of transport, convection, and the hydrologic cycle in chemical transport models: Implications for the modeling of short-lived and soluble species. *J. Geophys. Res. Atmos.*, 102(D23), pp. 28127-28138.
- Stein, T. H. M. et al., 2011. The vertical cloud structure of the West African monsoon: A 4 year climatology using CloudSat and CALIPSO. *J. Geophys. Res. Atmos.*, 116(D22205).
- Taylor, K. E., Stouffer, R. J. & Meehl, G. A., 2012. An Overview of CMIP5 and the Experiment Design. *Bull. Amer. Meteor. Soc.*, 93(4), pp. 485-498.
- Tselioudis, G., Rossow, W., Zhang, Y. & Konsta, D., 2013. Global Weather States and Their Properties from Passive and Active Satellite Cloud Retrievals. *Journal of Climate*, 26(19), pp. 7734-7746.

van der Linden, R., Fink, A. H. & Redl, R., 2015. Satellite-based climatology of low-level continental clouds in southern West Africa during the summer monsoon season. *J. Geophys. Res. Atmos.*, 120(3), pp. 1186-1201.

Waliser, D. E. et al., 2012. The "Year" of Tropical Convection (May 2008 to April 2010): Climate variability and weather highlights. *Bull. Amer. Meteor. Soc.*, 93(8), pp. 1189-1218.

Wang, J., Rossow, W. B. & Zhang, Y., 2000. Cloud Vertical Structure and Its Variations from a 20-Yr Global Rawinsonde Dataset. *Journal of Climate*, 13(17), pp. 3041-3056.

Wielicki, B. A. et al., 1996. Clouds and the Earth's Radiant Energy System (CERES): An Earth Observing System Experiment. *Bull. Amer. Meteor. Soc.*, 77(5), pp. 853-868.

Yu, H. et al., 2006. A review of measurement-based assessments of the aerosol direct radiative effect and forcing. *Atmos. Chem. Phys.*, Volume 6, pp. 613-666.